

Article

# Acoustic Emission-Based Detection of Impacts on Thermoplastic Aircraft Control Surfaces: A Preliminary Study

Li Ai <sup>1</sup>, Sydney Flowers <sup>2</sup>, Tanner Mesaric <sup>2</sup>, Bryson Henderson <sup>3</sup>, Sydney Houck <sup>3</sup> and Paul Ziehl <sup>1,3,\*</sup><sup>1</sup> Department of Civil and Environmental Engineering, University of South Carolina, Columbia, SC 29201, USA<sup>2</sup> Department of Integrated Information Technology, University of South Carolina, Columbia, SC 29201, USA<sup>3</sup> Department of Mechanical Engineering, University of South Carolina, Columbia, SC 29201, USA

\* Correspondence: ziehl@cec.sc.edu

**Abstract:** The reliability of aircraft control surfaces, constructed from thermoplastic materials, can be affected by impacts from airborne particles. Recognizing the exact position of such impacts is essential for correctly estimating the resulting damage. This research intended to address the issue by introducing an innovative structural health monitoring solution capable of autonomously detecting and localizing impacts using acoustic emission monitoring. The objective of this research is to investigate the application of AE for the localization of impacts on aircraft elevators using machine learning techniques, specifically regression algorithms. To achieve this goal, two algorithms, linear regression, and random forest, were employed for predicting the impact locations based on AE signals. The performance of each algorithm was validated on a thermoplastic composite aircraft elevator. Results indicated that both linear regression and random forest models show high accuracy in predicting the impact locations. The random forest model, with an  $R^2$  value of 0.98616 and an RMSE of 0.6778, outperformed the linear regression model, which exhibited an  $R^2$  value of 0.9361 and an RMSE of 1.4614.



**Citation:** Ai, L.; Flowers, S.; Mesaric, T.; Henderson, B.; Houck, S.; Ziehl, P. Acoustic Emission-Based Detection of Impacts on Thermoplastic Aircraft Control Surfaces: A Preliminary Study. *Appl. Sci.* **2023**, *13*, 6573. <https://doi.org/10.3390/app13116573>

Academic Editors: Victor Giurgiutiu and Kanji Ono

Received: 3 May 2023

Revised: 26 May 2023

Accepted: 26 May 2023

Published: 29 May 2023



**Copyright:** © 2023 by the authors. Licensee MDPI, Basel, Switzerland. This article is an open access article distributed under the terms and conditions of the Creative Commons Attribution (CC BY) license (<https://creativecommons.org/licenses/by/4.0/>).

**Keywords:** thermoplastic composite; impacts; acoustic emission; structural health monitoring

## 1. Introduction

The occurrence of impacts from random objects, such as ice particles and debris, presents a considerable obstacle in maintaining the structural integrity of composite components for aircraft systems. Conventionally, C-Scan inspections have been utilized for the appraisal of impact-induced damage [1–3]. However, this approach is prone to human inaccuracies, is time-consuming, and does not provide real-time results, as assessments can only be conducted between flight operations. The emergence of new sensor technologies and advanced data processing methods enables the deployment of structural health monitoring (SHM) systems [4–9]. Some SHM systems have the capacity to autonomously identify and evaluate impact damage while continuously monitoring aircraft components during flight operations [10–12]. As a result, reliance on labor-intensive and error-susceptible visual examinations may be diminished. The automated detection and localization of impact damage stemming from debris and hail through the incorporation of SHM systems offer a more timely, accurate, and efficient evaluation approach.

In recent years, various methods have been applied for SHM in aircraft structures. PZT sensors and vibration analysis are widely used due to their sensitivity to a broad frequency range and their ability to detect different types of damage [13]. Ultrasonic testing and guided wave techniques are also utilized due to their ability to inspect large areas of a structure [14]. However, it is noteworthy that each of these methods has its inherent limitations. For instance, the deployment of PZT sensors and the implementation of vibration analysis may necessitate intricate signal processing and interpretation, which may impose substantial complexity. Ultrasonic testing often demands direct contact with

the structure, a requirement that may not be practicable for aircraft in service, thereby restricting its usability in these contexts.

Acoustic emission (AE) monitoring is one SHM method worth investigating as it is a passive technique, detecting the energy released by the structure itself when it undergoes a change (e.g., impact or cracking) [15,16]. This allows for continuous, real-time monitoring without the need for external excitation. AE sensors can be mounted on the surface of the structure, making it a noninvasive and nondestructive method. Furthermore, AE has shown high sensitivity to various types of damage and can provide information about the damage's location and severity [17–20]. Several studies have explored the use of AE in monitoring damage to composites [21–26]. Barile et al. [23] utilized AE to identify the type of damage in carbon fiber-reinforced polymer (CFRP) samples by decomposing the AE signal using a Wavelet Packet Transform (WPT). Results showed that the signals could be categorized based on the type of damage mechanism. Similarly, Xu et al. [24] applied AE to unidirectional (UD) CFRP tendons and used Hilbert marginal energy spectrum (HMES) and instantaneous energy spectrum (IES) to identify damage patterns and evolution during tensioning. Mal et al. [25] studied the application of AE to assess the low-velocity impact (LVI) on fiber composites by applying AE to graphite–epoxy composite plates. Results showed that impact loads could be identified from the AE signals, and delamination could be assessed by examining the waveform of the recorded signal. James et al. [26] placed four AE sensors on CFRP specimens and conducted impact experiments. The AE waveforms and their corresponding frequency domain spectrum were analyzed to distinguish between different AE signatures, enabling the determination of whether the structure had been damaged due to impact events.

While the use of AE in monitoring the impact on fiber composite materials has shown promise, traditional methods of analyzing AE signals are often challenging, especially for complex datasets, and require manual analysis based on expertise. Furthermore, environmental restrictions during aircraft operations limit the number of AE sensors that can be attached to the aircraft, adding complexity to data analysis. Considering these limitations, developing approaches including machine learning are necessary to aid in the real-time analysis of AE data from a minimal number of sensors, in this case, a single AE sensor, and to discern impact locations.

Machine learning algorithms, such as support vector machines (SVM) [27], random forests [28], and artificial neural networks (ANN) [29], have been employed to classify AE signals into different classes and identify damage mechanisms and have demonstrated their ability to handle complex datasets and achieve acceptable accuracy in damage identification and damage localization in composite materials. For instance, Xu et al. [27] used SVM to classify AE signals obtained from carbon fiber-reinforced polymers, demonstrating the potential of machine learning in damage assessment. Wang et al. [28] employed random forests to identify the type and severity of defects in composite materials by analyzing AE signals. Ai et al. [29] investigated impact localizations on an aviation control surface. The localization task was considered a classification problem. ANN, random forest, and stacked autoencoder were used to classify AE data obtained from an impacted composite specimen into different regions and achieved acceptable accuracy.

The application of machine learning techniques for AE signal analysis in the previous literature highlighted the efficacy of these methods for the impact localization of aircraft control surfaces. Notably, existing research on impact localization of aircraft control surfaces using machine learning focuses on transforming impact localization into a classification problem, where the impact is confined to a relatively broad area. However, there is a gap in achieving accurate impact localization of aircraft control surfaces, specifically focusing on localizing impacts with precision instead of within a broad area. To address this gap, this paper presents a preliminary study that investigates the application of a single AE sensor for localizing impact on aircraft control surfaces. In this preliminary study, the impact energy is assumed to be constant. In contrast to treating localization as a classification issue, this approach employs two regression algorithms, namely, linear regression and random forest,

to accurately estimate the location of each impact event. Linear regression and random forest were chosen due to their simplicity and interpretability. The two methods provide a simple and effective way to model the relationship between the AE and impact locations. Moreover, linear regression and random forest models are computationally efficient, which is essential in a real-time SHM system. To assess the efficacy of the proposed method, an impact experiment was carried out on a specimen of an aircraft elevator. The findings of this research demonstrate that the proposed method effectively localizes impacts, thereby substantiating the potential of regression algorithms in enhancing the precision of impact localization for aircraft control surfaces.

## 2. Methods

### 2.1. Acoustic Emission Monitoring

Acoustic emission is a phenomenon that arises from the rapid release of energy within materials, giving rise to transient stress waves [30]. By positioning AE sensors on the surface of an object, it becomes possible to detect and gather acoustic emission (AE) signals [31]. The method of recording and processing AE signals to diagnose the health status of an object is referred to as AE monitoring. Through the analysis of the AE signal, it is feasible to extract various AE features. Schematic representations of commonly used AE features such as “Amplitude”, “Counts”, “Counts to peak”, “Rise time”, and “Duration” are shown in Figure 1.

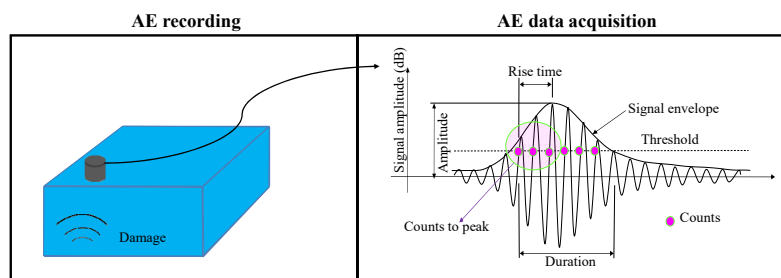


**Figure 1.** Acoustic emission monitoring (regenerated after [32]).

### 2.2. Impact Localization Using Linear Regression

Linear regression is a widely used technique for modeling the relationship between a dependent variable and one or more independent variables [33–35]. In this study, the dependent variable is the impact location, and the independent variables are features extracted from the AE signals. Linear regression works by fitting a linear equation to the observed data points in such a way that the sum of the squared differences between the actual and predicted values (residuals) is minimized. This process is known as Ordinary Least Squares (OLS) [36]. The linear equation can be expressed as follows:

$$y = \beta_0 + \beta_1 x_1 + \beta_2 x_2 + \dots + \beta_n x_n \quad (1)$$

where  $y$  refers to the dependent variable (impact location),  $\beta_0$  is the intercept (constant term), and  $\beta_1, \beta_2, \dots$ , and  $\beta_n$  are the coefficients of the independent variables  $x_1, x_2, \dots$ , and  $x_n$ .

### 2.3. Impact Localization Using Random Forest

Random forest is an ensemble learning method for classification and regression tasks [37]. It works by constructing multiple decision trees and combining their outputs to improve predictive accuracy and reduce overfitting [38]. The random forest algorithm consists of the following main steps: bootstrap sampling, tree construction, and aggregation [37].

In this study, both linear regression and random forest algorithms were applied to predict impact locations based on AE features. The performance of each method was

compared using various evaluation metrics, such as the coefficient of determination ( $R^2$ ) and root-mean-squared error (RMSE) [39]. This comparison aids in the determination of the most suitable model for prediction of impact locations in this specific context. Figure 2 presents the structure of a random forest regression model with 100 decision trees. The color circles in the figure refers to the node of decision trees.

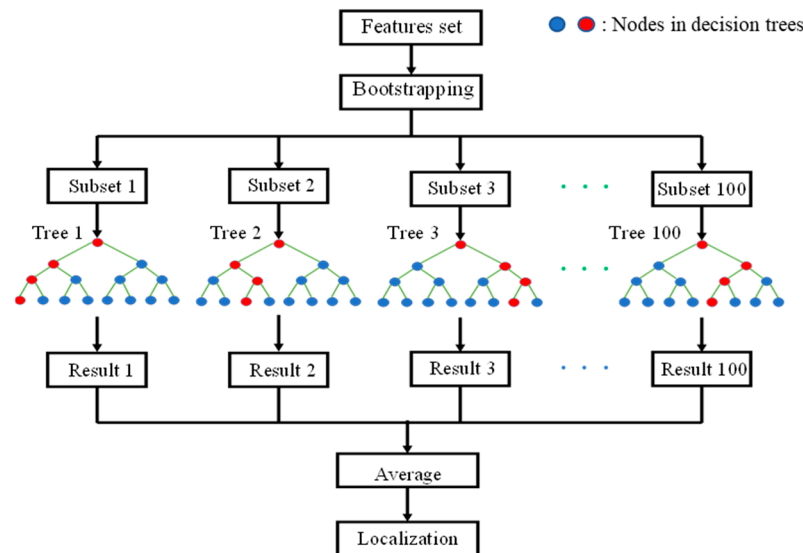


**Figure 2.** Structure of random forest regression model.

### 3. Experiment

#### 3.1. Specimen

To assess the efficacy of the impact localization methodologies delineated in this study, an impact experiment was conducted on an aircraft elevator from Gulfstream G650 [40]. The elevator was manufactured and provided by GKN Fokker. The elevator is a rib-stiffened box. On the top surface of the elevator, the panels are constructed in between the ribs. The elevator specimen was mounted on a 6.1 m long and 0.61 m high steel frame. The hinge brackets situated on the elevator spar were securely fastened to the corresponding hinge points on the frame. The elevator specimen is shown in Figure 3.

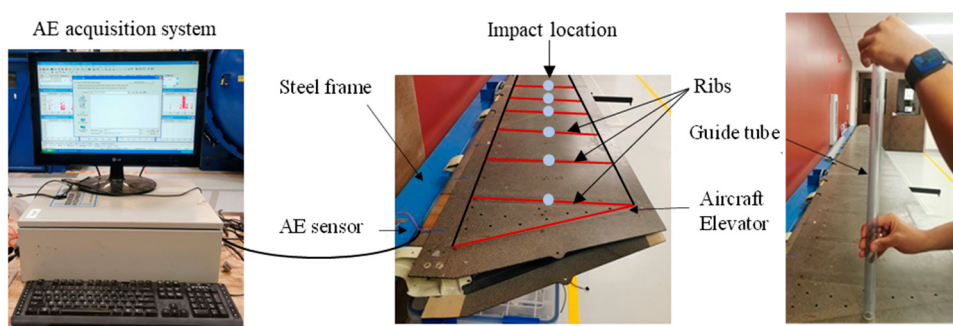


**Figure 3.** Impact experiment setup.

#### 3.2. Impact Experiment Setup

During the operation of aircraft, impacts may come from a range of sources, both natural and man-made. Among the natural sources, bird strikes and hailstorms pose a significant risk and are relatively frequent events in the aviation industry. These impacts may result in significant damage [41]. In terms of man-made sources, debris on runways also poses a significant risk. The debris can be propelled by the engines, causing potential damage to the fuselage or wings [42]. Of these sources, certain types of runway debris may

exhibit some degree of constant impact energy, assuming a degree of consistency between the type of debris, its size, and the speed of the aircraft during take-off or landing [43,44]. However, it is important to note that the inherent randomness and unpredictability of these phenomena often result in large variations in the associated impact energies. In order to simplify the impact scenario, the present paper only locates impacts of constant energy.

The impact experiment setup is shown in Figure 3. An experimental setup involving a steel sphere impacting the elevator specimen was employed to assess the proposed impact localization system. The steel sphere, with a diameter of 0.013 m and a weight of 8.4 g, was consistently positioned at 0.61 m from the elevator's surface for all impacts. The impact energy was maintained at 0.05 J, with all variables remaining constant except the impact location. A guide tube was utilized to regulate the location and height of each impact. The elevator featured 20 ribs, with one distinct impact point on each rib. An acoustic emission (AE) sensor was affixed to the elevator's spar near the location of the vertical stabilizer. This location was chosen to minimize cabling in the aircraft. Each impact location was subjected to 60 impacts, resulting in a total of 1200 impacts. AE signals were recorded by an acquisition system throughout the experiment. The dimensions, material of the elevator, and the locations of the sensor and impact are presented in Figure 4. It should be noted that in the rest of the paper, “rib number” is used as the label for linear regression and random forest models. This “rib numbering” refers to the listing of the ribs in Figure 4, starting from left to right.

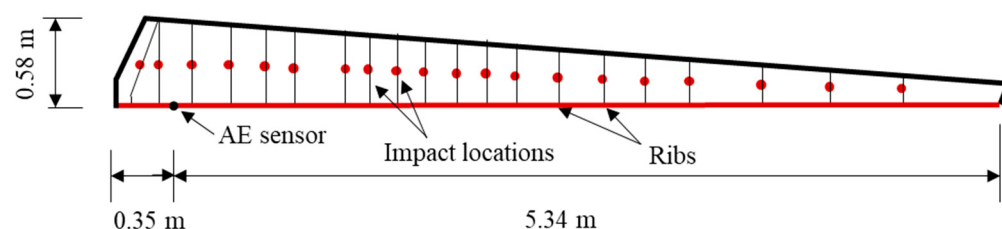


**Figure 4.** Dimensions of the elevator and the coordinates of impacts and sensor.

In this study, the impact of aircraft elevator panels was not investigated. As an integral part of the fuselage, the ribs are responsible for maintaining the aerodynamic shape of the control surfaces. Damage to the ribs due to impact (e.g., gradual reduction in stiffness due to repeated impacts) can therefore have serious aerodynamic and structural effects that may endanger flight safety. This investigation, therefore, prioritizes the monitoring of impacts to the ribs to facilitate a detailed understanding of their long-term structural integrity under repeated low-velocity impacts.

### 3.3. Acoustic Emission Data Acquisition

The AE system was purchased from MISTRAS Group Inc. (Princeton Junction, NJ, USA) and featured a PAC Micro-30 AE sensor with an operational frequency range of 150–400 kHz. The amplitude threshold was configured at 32 dB, with a sampling rate of 5 MHz. A pre-trigger time of 256  $\mu$ s was established to ensure the acquisition system captured the complete signal initiation. The peak definition time (PDT), representing the duration from threshold crossing to peak amplitude, was set at 200  $\mu$ s. A signal duration of 2000  $\mu$ s was employed to identify the peak, while the hit definition time (HDT)—governing the termination of impact recording—was configured at 400  $\mu$ s. Signal recording commenced when the voltage exceeded the threshold value and ceased when the HDT parameter duration elapsed without additional threshold crossings. Notably, the HDT is typically twice the PDT. Lastly, the hit lockout time (HLT) was established at 400  $\mu$ s to prevent the inclusion of reflected hits and late-arriving signals. All the parameters above for the acquisition system were defined according to the criteria in [32].

## 4. Results and Discussion

### 4.1. Acoustic Emission Data Preprocessing

As mentioned in the previous section, the AE signals for this study were obtained from an AE acquisition system during steel sphere impact testing. Figure 5 presents four typical AE signal waveforms recorded in the impact experiment. The difference in the AE waveform pattern can be related to the difference in the impact location and the distance between the sensors. AE signals were subsequently processed to extract relevant features from the AE waveform. The purpose of extracting these features was to distill the complex information embedded within the signal into a set of specific, representative values that effectively capture the properties of the AE signal. In the present study, a total of 15 key features, including count, signal strength, and reverberation frequency, were derived from the initial signal. Count refers to the number of threshold crossings in the AE signal. In simpler terms, it is a measure of how many times the signal goes beyond a certain predefined limit, which can indicate the intensity of the emission. Signal strength is essentially the integral of the rectified voltage signal over the waveform duration. It provides a quantitative measure of the overall “energy” present in the AE signal. This feature is essential in understanding the severity of the impact or event causing the emission. Reverberation frequency is the frequency after the peak of the AE signal. Essentially, it is the dominant frequency that persists after the initial, most intense portion of the signal has passed. This feature can provide insights into the nature of the event causing the emission, as different events can have different reverberation characteristics.

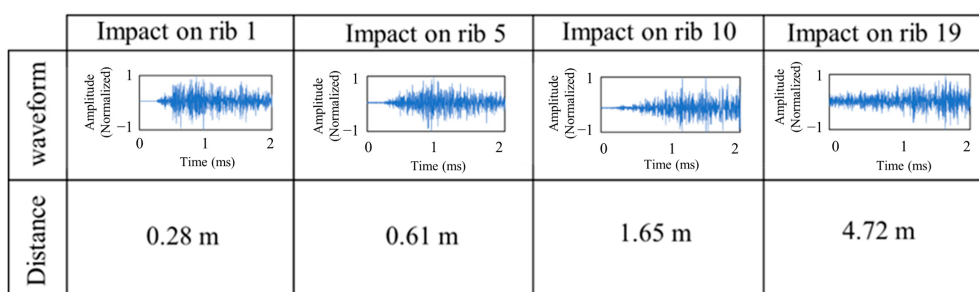


**Figure 5.** The typical AE waveforms generated by the impact.

A comprehensive list of all features, along with their descriptions, is provided in Table 1. These 15 features were selected as they have shown the good performance of source locations [17]. The linear regression and random forest models proposed in this study were applied to an input dataset composed of 1200 samples, each encompassing all 15 extracted features.

**Table 1.** AE features and their descriptions.

Parametric Features	Feature Descriptions
Amplitude	The highest magnitude observed in the AE waveform.
Average signal level (ASL)	The effective voltage with a characteristic time $T_{ASL}$ .
Root mean square (RMS)	The effective voltage with a characteristic time $T_{RMS}$ .
Energy	Quantification of the electrical energy contained within an AE signal.
Signal strength	The integral of the rectified voltage signal over the waveform duration.
Absolute energy	The absolute magnitude of electrical energy measured in an AE signal.
Rise time	The duration between the initial threshold crossing and the peak.
Duration	The time span encompassing the first and last threshold crossings.
Count	The count of instances where the signal crosses a predefined threshold.
Counts to peak (PCNTS)	The number of threshold crossings from the first crossing to the peak.
Average frequency	A parameter used to describe the overall frequency content of an AE signal.
Peak frequency	The frequency at which the signal exhibits its highest contribution.
Frequency centroid	A parameter used to characterize the overall frequency distribution or spectral content of an AE signal.
Reverberation frequency	The dominant frequency that persists after the initial, most intense portion of the signal has passed.
Initial frequency	The dominant frequency observed before the peak.

#### 4.2. Localization Results Using Linear Regression

Before inputting all 15 AE features into the linear regression model, feature analysis was performed by computing the correlation coefficient. The correlation coefficient is a numerical value that measures the strength and direction of a linear relationship between two variables. It is a descriptive value that is used heavily in statistics to make conclusions about data. The coefficient can range from  $-1$  to  $1$ , and the closer the coefficient is to either  $-1$  or  $1$ , the stronger the relationship between variables. We utilized this technique to identify potentially relevant features and subsequently plot a Pearson correlation heatmap (Figure 6) for visualization purposes. Upon examining the correlations between the AE feature and the impact location (rib number), several significant relationships are observed. The strongest negative correlation is with amplitude ( $-0.9302$ ), suggesting an inverse relationship between it and the rib number. As amplitude increases, the rib number tends to decrease, indicating that amplitude is a critical factor in determining the impact location. Other features, such as duration ( $-0.7022$ ), count ( $-0.6845$ ), and average frequency ( $-0.7199$ ), also exhibit strong negative correlations with the rib number, highlighting their potential correlation with the impact locations. Conversely, rise time ( $0.3463$ ) demonstrates a moderate positive correlation with rib number, implying that higher rise time values correspond to higher rib number. When looking at the five frequency-related parameters used (reverberation frequency, average frequency, peak frequency, initial frequency, and frequency centroid), the reverberation frequency and the average frequency are the parameters of more prominent relevance. The reverberation frequency is defined as the frequency of a signal after reflection from various structural boundaries, and it conveys a wealth of information about the geometry of the structure and the AE wave propagation path. This information becomes indispensable when the task is to locate the AE source with a single sensor [45,46]. The average frequency, another frequency parameter with high correlation, contains the reverberation frequency. Thus, both the reverberation frequency and the average frequency have a high correlation with the impact location. In contrast, the peak and initial frequencies and frequency centroid contain no information about the reverberation. These parameters encapsulate different sides of the AE signal and, unlike reverberant frequencies, have no propagation path or structural boundary effects. Therefore, they have a much lower correlation with the impact location.



**Figure 6.** Heat map of correction coefficients.

The correlation coefficients presented between the features and the label offer critical insights into the relationships that may be leveraged when selecting features for a linear regression model. In developing an accurate and reliable model, it is essential to select features that exhibit a strong correlation with the label, while minimizing multicollinearity among the selected features. The absolute values of the correlation coefficients between the impact location and the 15 AE features are shown in Figure 7. All correlation coefficients are arranged in ascending order.

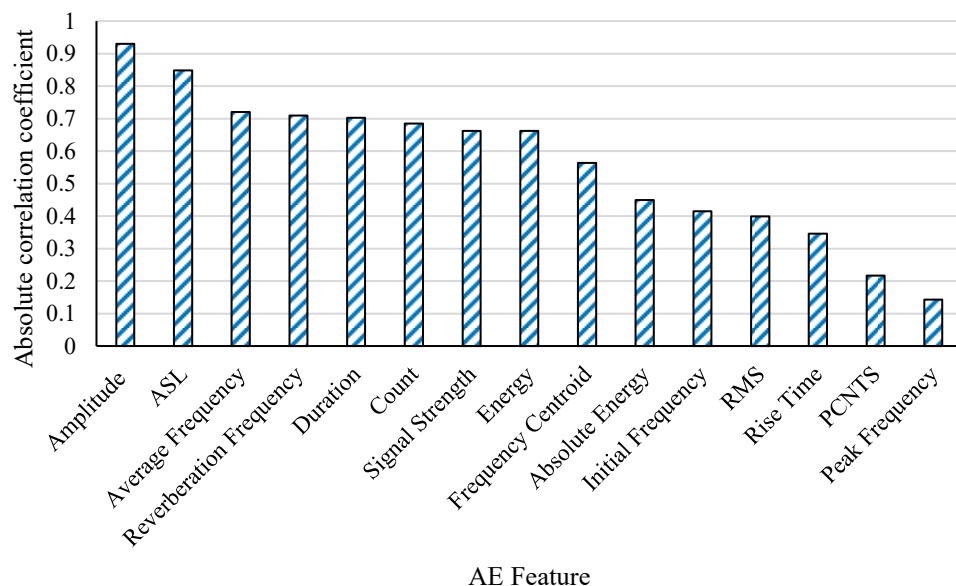


**Figure 7.** The rank of features in ascending order.

For the linear regression model in this paper, the learning rate is set as 0.1, and the max iteration is 1000. Following the ranking of features based on their correlations, a backward elimination process was employed, iteratively removing the feature with the lowest ranking, and subsequently utilizing the remaining features in the linear regression model. The RMSE and  $R^2$  values were computed at each step to evaluate the performance of the model. Tables 2 and 3 display the coefficients of all features used in constructing the linear regression equation, as well as the corresponding  $R^2$  and RMSE values obtained when each feature is sequentially deleted. Initially, the model demonstrated a high  $R^2$  value of 0.9361 and a low RMSE of 1.4614. As features were progressively removed, the  $R^2$  value gradually decreased, and the RMSE increased, indicating a reduction in the model's explanatory power and accuracy. It should be noted that the  $R^2$  value remained stable until the ninth feature was removed, after which a more significant decline was observed. This suggests that the first eight features removed had a comparatively limited impact on the performance of the linear regression model, and the remaining features were more influential in predicting the label. In summary, these findings suggest that all features contribute to the prediction of the impact location and should be retained in the linear regression model.

**Table 2.** Coefficients of features used in the linear regression equation, and  $R^2$  and RMSE for backward elimination.

Coefficients of Variables	Delete None	Delete 1	Delete 2	Delete 3	Delete 4	Delete 5	Delete 6
Amplitude	−0.38874	−0.40864	−0.40198	−0.43819	−0.4686	−0.47675	−0.47685
ASL	−0.14194	−0.18554	−0.1897	−0.19827	−0.10552	−0.1097	−0.11016
Average Frequency	0.054975	−0.28685	−0.30435	−0.02979	−0.02353	−0.02833	−0.02848
Reverberation Frequency	−0.0445	0.28347	0.296833	0.035397	0.033767	0.042611	0.042782
Duration	$1.56 \times 10^{-5}$	$-6.00 \times 10^{-6}$	$-2.00 \times 10^{-5}$	$1.37 \times 10^{-5}$	$1.48 \times 10^{-5}$	$2.34 \times 10^{-5}$	$2.31 \times 10^{-5}$
Count	−0.00236	−0.00195	−0.00168	−0.00228	−0.00215	−0.00231	−0.00232
Signal Strength	$-6.30 \times 10^{-6}$	$-6.40 \times 10^{-6}$	$-7.50 \times 10^{-6}$	$-2.00 \times 10^{-6}$	$-4.70 \times 10^{-6}$	$-1.50 \times 10^{-6}$	$-1.50 \times 10^{-6}$
Energy	−0.66253	0.054989	0.060861	0.02966	0.043758	0.024108	0.024254
Frequency Centroid	−0.02227	−0.03006	−0.01738	−0.03135	−0.03521	−0.03764	−0.03763
Absolute Energy	$-2.30 \times 10^{-6}$	$-9.00 \times 10^{-7}$	$-3.50 \times 10^{-7}$	$-1.10 \times 10^{-6}$	$8.92 \times 10^{-8}$	$5.72 \times 10^{-8}$	/
Initial Frequency	0.000384	−0.00117	−0.0014	−0.00319	−0.00323	/	/
RMS	33.16985	65.97887	66.95417	50.09611	/	/	/
Rise Time	0.00504	0.001808	0.001882	/	/	/	/
PCNTS	0.010839	0.014069	/	/	/	/	/
Peak Frequency	−0.05168	/	/	/	/	/	/
Intercept	36.09853	39.63695	39.70405	43.43703	43.1448	43.42157	43.43426
$R^2$	0.9361	0.9281	0.9255	0.9197	0.9187	0.9176	0.9176
RMSE	1.4614	1.5507	1.5784	1.6390	1.6485	1.6599	1.6599

**Table 3.** Continuation of Table 2.

Coefficients of Variables	Delete 7	Delete 8	Delete 9	Delete 10	Delete 11	Delete 12	Delete 13
Amplitude	−0.53962	−0.53972	−0.54393	−0.58384	−0.60369	−0.60258	−0.59833
ASL	−0.04556	−0.04548	0.201282	0.235985	0.230852	0.229102	0.228328
Average Frequency	0.002124	0.002091	−0.0418	−0.03239	0.012376	0.004003	/
Reverberation Frequency	0.019079	0.019156	0.017189	0.037602	−0.00845	/	/
Duration	$5.61 \times 10^{-5}$	$5.63 \times 10^{-5}$	−0.00013	$-3.50 \times 10^{-5}$	/	/	/
Count	−0.00284	−0.00284	0.001274	/	/	/	/
Signal Strength	$-4.50 \times 10^{-6}$	$2.37 \times 10^{-6}$	/	/	/	/	/
Energy	0.042939	/	/	/	/	/	/
Frequency Centroid	/	/	/	/	/	/	/
Absolute Energy	/	/	/	/	/	/	/
Initial Frequency	/	/	/	/	/	/	/
RMS	/	/	/	/	/	/	/
Rise Time	/	/	/	/	/	/	/
PCNTS	/	/	/	/	/	/	/
Peak Frequency	/	/	/	/	/	/	/
Intercept	−0.53962	−0.53972	−0.54393	−0.58384	−0.60369	−0.60258	−0.59833
$R^2$	0.9115	0.9115	0.8784	0.8774	0.8757	0.8757	0.8757
RMSE	1.7198	1.7199	2.0162	2.0247	2.0386	2.0387	2.0390

#### 4.3. Localization Results Using Random Forest

For the random forest model in this paper, the base model is classification and regression trees (CART). The split criteria are mean square error MSE. The number of random features to consider at each split is set as 5. Prior to employing the random forest model for predicting impact locations, it is crucial to optimize the number of decision trees involved in the model. In this study, an exploratory trial-and-error experiment was conducted to

optimize the random forest model by incrementally increasing the number of decision trees, ranging from 1 to 200, while examining the out-of-bag (OOB) error. The OOB error serves as a valuable metric for evaluating the random forest model during the training phase. For each decision tree within the random forest, a random subset of the training data is selected and employed to construct the tree, while the remaining data points are utilized for calculating the OOB error. The OOB error effectively measures the proportion of misclassified samples among the OOB samples for a given decision tree.

For localization of impact, the OOB error is the ratio of accurately located impacts to the total number of impacts. The random forest-predicted impact locations are rounded and then compared to the actual impact locations. To enable a meaningful comparison between the predicted impact locations and their actual counterparts, the random forest model's predictions are rounded to the nearest integer values. The OOB error analysis revealed that the model attained the minimum OOB error (18.19%) when approximately 100 decision trees were incorporated. Consequently, a random forest model comprising 100 trees was selected for the remainder of this study. This optimization process ensures that the model achieves a balance between complexity and generalizability, minimizing the risk of overfitting while maximizing predictive performance.

Upon optimizing the number of decision trees, the AE dataset, consisting of 15 features, was incorporated into the random forest model as input. The dataset was partitioned using a 70/30 training/testing ratio to ensure a robust evaluation of the performance. The results demonstrated a high level of accuracy, indicating that the model is well suited for the given task. Figure 8 illustrates a comparison of the actual impact locations with their corresponding predicted impact locations derived from the model. The  $R^2$  value, equal to 0.98616, signifies a good fit between the predictions and the actual labels. This suggests that the model is adept at accurately capturing the underlying relationships between the predictor variables and the response variable.

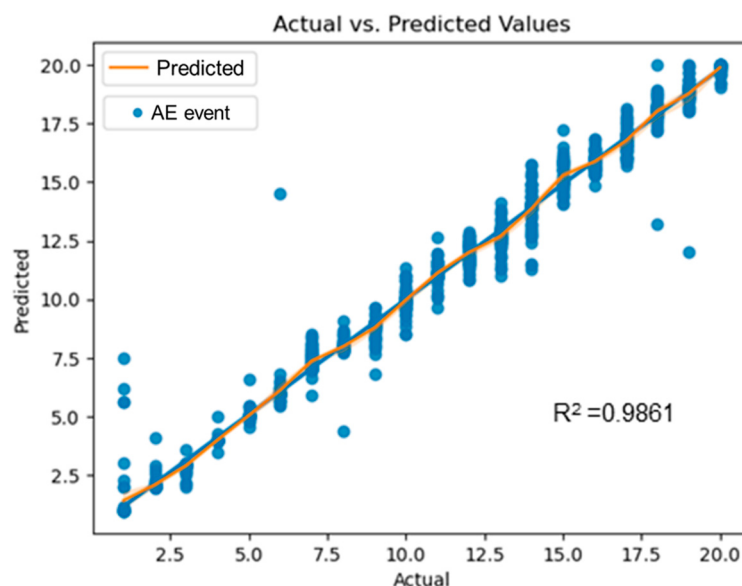


**Figure 8.** Random forest result—actual impact locations versus predicted impact locations.

Figure 9 presents a comparative analysis of the true impact locations and their respective model-generated predictions. Upon closer examination, it is evident that the discrepancies between the predicted values and the actual labels are minor, signifying a high degree of accuracy in the performance. To quantify these errors more rigorously and evaluate the reliability, the RMSE was calculated. In this case, the random forest model boasts a notably low RMSE value of 0.6778, which further substantiates its accuracy and precision. The findings of  $R^2$  and RMSE suggest that the predictions align closely with the

actual impact locations, making the random forest model a dependable tool for locating the impact location within the confines of this study.

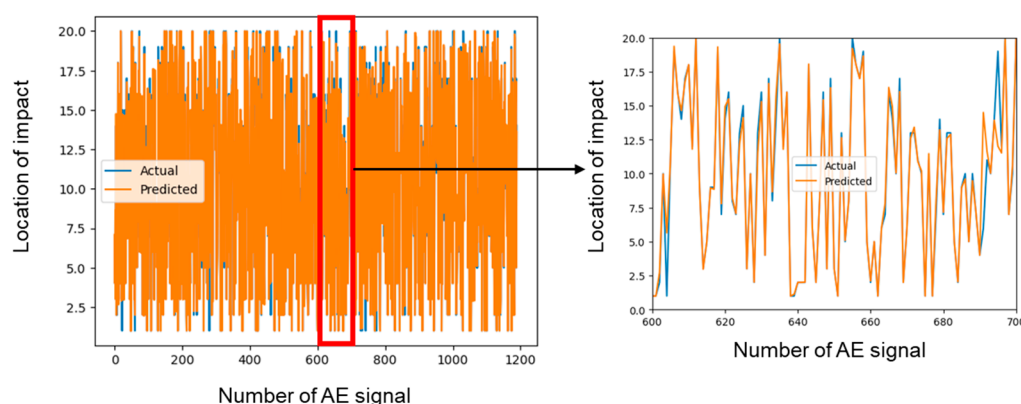


**Figure 9.** The comparison of actual impact locations and predicted impact locations.

## 5. Conclusions

This study investigated the use of AE monitoring for impact localization on aircraft elevators, employing two regression machine learning models—linear regression and random forest—to analyze AE signals and predict impact locations. The study demonstrated the efficacy of both models, with the random forest model outperforming the linear regression model in terms of accuracy. The key findings and conclusions drawn are as follows:

1. AE monitoring has the potential to be an effective tool for detecting and localizing impacts on aircraft elevators, offering a real-time and noninvasive monitoring solution for improved aircraft safety and maintenance.
2. Both linear regression and random forest regression models demonstrated high accuracy in predicting impact locations, proving the effectiveness of regression algorithms in analyzing AE signals for impact localization.
3. The Pearson correlation analysis demonstrated a strong correlation between amplitude and impact location, suggesting that amplitude may be a critical factor in predicting the impact location using linear regression.
4. The random forest model demonstrated better performance compared to the linear regression model, with a higher  $R^2$  value (0.98616) and a lower RMSE (0.6778), indicating its potential for practical applications in the aviation industry.

The limitation of the current study is the difficulty with access to the labeled AE signals for existing aircraft components. Future studies may address this issue by employing transfer learning or involving simulation AE data in the training of machine learning models. Future research could also explore other machine learning models and feature extraction methods to further enhance the accuracy of impact localization on aircraft elevators using AE monitoring, as well as investigate the scalability of these techniques to other parts of the aircraft. By incorporating additional sensor data, such as strain and temperature measurements, future research could also further improve the accuracy and reliability of the impact localization system, providing a more holistic understanding of structural health.

**Author Contributions:** Conceptualization, L.A. and P.Z.; methodology, L.A., S.F. and T.M.; software, L.A., S.F. and T.M.; formal analysis, L.A., S.F. and T.M.; data curation, L.A., B.H. and S.H.; writing—original draft preparation, L.A., S.F. and T.M.; writing—review and editing, P.Z.; supervision, L.A. and P.Z.; project administration, P.Z.; funding acquisition, P.Z. All authors have read and agreed to the published version of the manuscript.

**Funding:** This research was conducted at the University of South Carolina and was partially funded through the NASA University Leadership Initiative Cooperative Agreement entitled Innovative

Manufacturing, Operation, and Certification of Advanced Structures for Civil Vertical Lift Vehicles led by Georgia Tech, Agreement No. 80NSSC21M0113. The APC was waived. The NASA technical monitor is Emilie Siochi. Opinions, interpretations, conclusions, and recommendations are those of the authors and are not necessarily endorsed by the United States Government.

**Institutional Review Board Statement:** Not applicable.

**Informed Consent Statement:** Not applicable.

**Data Availability Statement:** The raw/processed data required to reproduce these findings will be made available on request.

**Conflicts of Interest:** The authors declare no conflict of interest.

## References

- Riccio, A.; Saputo, S.; Sellitto, A.; Lopresto, V. Characterization of the impact induced damage in composites by cross-comparison among experimental non-destructive evaluation techniques and numerical simulations. *Proc. Inst. Mech. Eng. Part C J. Mech. Eng. Sci.* **2017**, *231*, 3077–3090. [[CrossRef](#)]
- Habibi, M.; Laperrière, L.; Hassanabadi, H.M. Influence of low-velocity impact on residual tensile properties of nonwoven flax/epoxy composite. *Compos. Struct.* **2018**, *186*, 175–182. [[CrossRef](#)]
- Tian, Z.; Yu, L.; Leckey, C.; Seebo, J. Guided wave imaging for detection and evaluation of impact-induced delamination in composites. *Smart Mater. Struct.* **2015**, *24*, 105019. [[CrossRef](#)]
- Garrett, J.C.; Mei, H.; Giurgiutiu, V. An Artificial Intelligence Approach to Fatigue Crack Length Estimation from Acoustic Emission Waves in Thin Metallic Plates. *Appl. Sci.* **2022**, *12*, 1372. [[CrossRef](#)]
- Giannakeas, I.N.; Khodaei, Z.S.; Aliabadi, M. Digital clone testing platform for the assessment of SHM systems under uncertainty. *Mech. Syst. Signal Process.* **2022**, *163*, 108150. [[CrossRef](#)]
- Ai, L.; Zhang, B.; Ziehl, P. A transfer learning approach for acoustic emission zonal localization on steel plate-like structure using numerical simulation and unsupervised domain adaptation. *Mech. Syst. Signal Process.* **2023**, *192*, 110216. [[CrossRef](#)]
- Laxman, K.; Tabassum, N.; Ai, L.; Cole, C.; Ziehl, P. Automated crack detection and crack depth prediction for reinforced concrete structures using deep learning. *Constr. Build. Mater.* **2023**, *370*, 130709. [[CrossRef](#)]
- Tan, X.; Abu-Obeidah, A.; Bao, Y.; Nassif, H.; Nasreddine, W. Measurement and visualization of strains and cracks in CFRP post-tensioned fiber reinforced concrete beams using distributed fiber optic sensors. *Autom. Constr.* **2021**, *124*, 103604. [[CrossRef](#)]
- Tan, X.; Bao, Y. Measuring crack width using a distributed fiber optic sensor based on optical frequency domain reflectometry. *Measurement* **2021**, *172*, 108945. [[CrossRef](#)]
- Alvarez-Montoya, J.; Carvajal-Castrillón, A.; Sierra-Pérez, J. In-flight and wireless damage detection in a UAV composite wing using fiber optic sensors and strain field pattern recognition. *Mech. Syst. Signal Process.* **2020**, *136*, 106526. [[CrossRef](#)]
- Rocha, H.; Semprimoschnig, C.; Nunes, J.P. Sensors for process and structural health monitoring of aerospace composites: A review. *Eng. Struct.* **2021**, *237*, 112231. [[CrossRef](#)]
- Migot, A.; Mei, H.; Giurgiutiu, V. Numerical and experimental investigation of delaminations in a unidirectional composite plate using NDT and SHM techniques. *J. Intell. Mater. Syst. Struct.* **2021**, *32*, 1781–1799. [[CrossRef](#)]
- Salmanpour, M.S.; Khodaei, Z.S.; Aliabadi, M.H.F. Impact Damage Localization with Piezoelectric Sensors under Operational and Environmental Conditions. *Sensors* **2017**, *17*, 1178. [[CrossRef](#)]
- Ochôa, P.; Groves, R.M.; Benedictus, R. Systematic multiparameter design methodology for an ultrasonic health monitoring system for full-scale composite aircraft primary structures. *Struct. Control. Health Monit.* **2019**, *26*, e2340. [[CrossRef](#)]
- Ono, K. Application of acoustic emission for structure diagnosis. *Diagnostyka* **2011**, *2*, 3–18.
- Ono, K. Review on Structural Health Evaluation with Acoustic Emission. *Appl. Sci.* **2018**, *8*, 958. [[CrossRef](#)]
- Ai, L.; Soltangharaei, V.; Bayat, M.; Greer, B.; Ziehl, P. Source localization on large-scale canisters for used nuclear fuel storage using optimal number of acoustic emission sensors. *Nucl. Eng. Des.* **2021**, *375*, 111097. [[CrossRef](#)]
- Soltangharaei, V.; Anay, R.; Ai, L.; Giannini, E.R.; Zhu, J.; Ziehl, P. Temporal Evaluation of ASR Cracking in Concrete Specimens Using Acoustic Emission. *J. Mater. Civ. Eng.* **2020**, *32*, 04020285. [[CrossRef](#)]
- Laxman, K.C.; Ross, A.; Ai, L.; Henderson, A.; Elbatanouny, E.; Bayat, M.; Ziehl, P. Determination of vehicle loads on bridges by acoustic emission and an improved ensemble artificial neural network. *Constr. Build. Mater.* **2023**, *364*, 129844. [[CrossRef](#)]
- Ai, L.; Soltangharaei, V.; Ziehl, P. Developing a heterogeneous ensemble learning framework to evaluate Alkali-silica reaction damage in concrete using acoustic emission signals. *Mech. Syst. Signal Process.* **2022**, *172*, 108981. [[CrossRef](#)]
- Ono, K.; Gallego, A. Research and applications of AE on advanced composites. *J. Acoust. Emiss.* **2012**, *30*, 180–229.
- Ai, L.; Soltangharaei, V.; Anay, R.; van Tooren, M.J.; Ziehl, P. Data-Driven Source Localization of Impact on Aircraft Control Surfaces. In Proceedings of the 2020 IEEE Aerospace Conference, Big Sky, MT, USA, 7–14 March 2020. [[CrossRef](#)]
- Barile, C.; Casavola, C.; Pappalettera, G.; Vimalathithan, P.K. Damage characterization in composite materials using acoustic emission signal-based and parameter-based data. *Compos. Part B Eng.* **2019**, *178*, 107469. [[CrossRef](#)]
- Xu, J.; Wang, W.; Han, Q.; Liu, X. Damage pattern recognition and damage evolution analysis of unidirectional CFRP tendons under tensile loading using acoustic emission technology. *Compos. Struct.* **2020**, *238*, 111948. [[CrossRef](#)]

25. Mal, A.K.; Shih, F.; Banerjee, S. Acoustic emission waveforms in composite laminates under low velocity impact. In Proceedings of the NDE for health monitoring and diagnostics, San Diego, CA, USA, 2–6 March 2003. [[CrossRef](#)]
26. James, R.; Joseph, R.P.; Giurgiutiu, V. Impact damage ascertainment in composite plates using in-situ acoustic emission signal signature identification. *J. Compos. Sci.* **2021**, *5*, 79. [[CrossRef](#)]
27. Xu, J.; Liu, X.; Han, Q.; Wang, W. A particle swarm optimization–support vector machine hybrid system with acoustic emission on damage degree judgment of carbon fiber reinforced polymer cables. *Struct. Health Monit.* **2021**, *20*, 1551–1562. [[CrossRef](#)]
28. Wang, Z.; Chegdani, F.; Yalamarti, N.; Takabi, B.; Tai, B.; El Mansori, M.; Bukkapatnam, S. Acoustic emission characterization of natural fiber reinforced plastic composite machining using a random forest machine learning model. *J. Manuf. Sci. Eng.* **2020**, *142*, 031003. [[CrossRef](#)]
29. Ai, L.; Soltangharaei, V.; Bayat, M.; van Tooren, M.; Ziehl, P. Detection of impact on aircraft composite structure using machine learning techniques. *Meas. Sci. Technol.* **2021**, *32*, 084013. [[CrossRef](#)]
30. Soltangharaei, V.; Ai, L.; Anay, R.; Bayat, M.; Ziehl, P. Implementation of Information Entropy, b-Value, and Regression Analyses for Temporal Evaluation of Acoustic Emission Data Recorded during ASR Cracking. *Pract. Period. Struct. Des. Constr.* **2021**, *26*, 04020065. [[CrossRef](#)]
31. Ai, L.; Soltangharaei, V.; Ziehl, P. Evaluation of ASR in concrete using acoustic emission and deep learning. *Nucl. Eng. Des.* **2021**, *380*, 111328. [[CrossRef](#)]
32. Unnþórssón, R. Hit detection and determination in AE bursts. *Acoust. Emiss.-Res. Appl.* **2013**, 1–20.
33. Su, X.; Yan, X.; Tsai, C.L. Linear regression. *Wiley Interdiscip. Rev. Comput. Stat.* **2012**, *4*, 275–294. [[CrossRef](#)]
34. Uyanik, G.K.; Güler, N. A Study on Multiple Linear Regression Analysis. *Procedia—Soc. Behav. Sci.* **2013**, *106*, 234–240. [[CrossRef](#)]
35. Maulud, D.; AbdulAzeez, A.M. A Review on Linear Regression Comprehensive in Machine Learning. *J. Appl. Sci. Technol. Trends* **2020**, *1*, 140–147. [[CrossRef](#)]
36. Craven, B.; Islam, S.M. Ordinary least-squares regression. *SAGE Dict. Quant. Manag. Res.* **2011**, 224–228.
37. Breiman, L. Random forests. *Mach. Learn.* **2001**, *45*, 5–32. [[CrossRef](#)]
38. Genuer, R.; Poggi, J.-M.; Tuleau-Malot, C. Variable selection using random forests. *Pattern Recognit. Lett.* **2010**, *31*, 2225–2236. [[CrossRef](#)]
39. Ai, L.; Bayat, M.; Ziehl, P. Localizing damage on stainless steel structures using acoustic emission signals and weighted ensemble regression-based convolutional neural network. *Measurement* **2023**, *211*, 112659. [[CrossRef](#)]
40. Van Ingen, J.W.; Buitenhuis, A.; Van Wijngaarden, M.; Simmons, F. Development of the Gulfstream G650 induction welded thermoplastic elevators and rudder. In Proceedings of the International SAMPE Symposium and Exhibition, Seattle, WA, USA, 23–28 May 2010.
41. Allan, J.R. The costs of bird strikes and bird strike prevention. *Hum. Confl. Wildl. Econ. Consid.* **2000**, 18.
42. Nguyen, S.N.; Greenhalgh, E.S.; Graham, J.M.R.; Francis, A.; Olsson, R. Runway debris impact threat maps for transport aircraft. *Aeronaut. J.* **2014**, *118*, 229–266. [[CrossRef](#)]
43. Greenhalgh, E.S.; Chichester, G.A.F.; Mew, A.; Slade, M.; Bowen, R. Characterization of the realistic impact threat from runway debris. *Aeronaut. J.* **2001**, *105*, 557–570. [[CrossRef](#)]
44. Nguyen, S.N.; Greenhalgh, E.S.; Olsson, R.; Iannucci, L.; Curtis, P.T. Modeling the Lofting of Runway Debris by Aircraft Tires. *J. Aircr.* **2008**, *45*, 1701–1714. [[CrossRef](#)]
45. Ebrahimkhanlou, A.; Dubuc, B.; Salamone, S. A generalizable deep learning framework for localizing and characterizing acoustic emission sources in riveted metallic panels. *Mech. Syst. Signal Process.* **2019**, *130*, 248–272. [[CrossRef](#)]
46. Ebrahimkhanlou, A.; Dubuc, B.; Salamone, S. Damage localization in metallic plate structures using edge-reflected lamb waves. *Smart Mater. Struct.* **2016**, *25*, 085035. [[CrossRef](#)]

**Disclaimer/Publisher’s Note:** The statements, opinions and data contained in all publications are solely those of the individual author(s) and contributor(s) and not of MDPI and/or the editor(s). MDPI and/or the editor(s) disclaim responsibility for any injury to people or property resulting from any ideas, methods, instructions or products referred to in the content.